Biosensors and Bioelectronics 177 (2021) 112887

Contents lists available at ScienceDirect

Biosensors and Bioelectronics

journal homepage: http://www.elsevier.com/locate/bios

CRISPR-powered electrochemical microfluidic multiplexed biosensor for target amplification-free miRNA diagnostics

Richard Bruch [a,b], Midori Johnston [a,b], André Kling [c], Thorsten Mattmüller [a], Julia Baaske [d], Stefan Partel [e], Sibylle Madlener [f], Wilfried Weber [d], Gerald A. Urban [a,g], Can Dincer [a,b,*]

[a] University of Freiburg, Department of Microsystems Engineering, Germany
[b] University of Freiburg, Freiburg Center for Interactive Materials and Bioinspired Technologies, Germany
[c] ETH Zurich, Department of Biosystems Science and Engineering, Switzerland
[d] University of Freiburg, Faculty of Biology and Signalling Research Centers BIOSS and CIBSS, Germany
[e] Vorarlberg University of Applied Sciences, Research Center of Microtechnology, Austria
[f] Medical University of Vienna, Department of Pediatrics and Adolescent Medicine, Austria
[g] University of Freiburg, Freiburg Materials Research Center, Germany

ARTICLE INFO

Keywords:
CRISPR/Cas technology
MicroRNA analysis
Electrochemical biosensors
Multiplexed microfluidics
Point-of-care testing

ABSTRACT

Recently the use of microRNAs (miRNAs) as biomarkers for a multitude of diseases has gained substantial significance for clinical as well as point-of-care diagnostics. Amongst other challenges, however, it holds the central requirement that the concentration of a given miRNA must be evaluated within the context of other factors in order to unambiguously diagnose one specific disease. In terms of the development of diagnostic methods and devices, this implies an inevitable demand for multiplexing in order to be able to gauge the abundance of several components of interest in a patient's sample in parallel. In this study, we design and implement different multiplexed versions of our electrochemical microfluidic biosensor by dividing its channel into subsections, creating four novel chip designs for the amplification-free and simultaneous quantification of up to eight miRNAs on the CRISPR-Biosensor X ('X' highlighting the multiplexing aspect of the device). We then use a one-step model assay followed by amperometric readout in combination with a 2-min-stop-flow-protocol to explore the fluidic and mechanical characteristics and limitations of the different versions of the device. The sensor showing the best performance, is subsequently used for the Cas13a-powered proof-of-concept measurement of two miRNAs (miRNA-19b and miRNA-20a) from the miRNA-17–92 cluster, which is dysregulated in the blood of pediatric medulloblastoma patients. Quantification of the latter, alongside simultaneous negative control measurements are accomplished on the same device. We thereby confirm the applicability of our platform to the challenge of amplification-free, parallel detection of multiple nucleic acids.

1. Introduction

An increasing number of studies have documented the emergence of dysregulated, circulating microRNAs (miRNAs) as biomarkers for various diseases such as cancer (Palanichamy and Rao, 2014), Huntington's disease (Johnson et al., 2008) and psychiatric diseases (Miller and Wahlestedt, 2010). These short (18–25 nucleotides) non-coding oligonucleotides are involved in the regulation of a wide range of physiological processes through degradation or translational repression of their target messenger RNAs (mRNAs) (Bartel, 2009) and may also impact their structure and interaction with proteins (Filipowicz et al., 2008). Therefore, dysregulation of miRNAs, and hence aberrant abundance in human body fluids, (blood, saliva or cerebrospinal fluid (Chen et al., 2008; Handy et al., 2011; Perdaens et al., 2020)), is being investigated as a novel, non- or minimally invasive diagnostic biomarker (Cheng, 2015).

However, to this date, it is impossible to accurately and unambiguously diagnose a particular illness by merely assessing the incidence of one specific dysregulated 'signature' miRNA within a clinical sample. Also, there is no commonly accepted standard for the interpretation of miRNAs as biomarkers. This is partially due to the fact that each miRNA is estimated to target hundreds of transcripts (Friedman and Jones,

* Corresponding author. University of Freiburg, FIT – Freiburg Center for Interactive Materials and Bioinspired Technologies, Georges-Köhler-Allee 105, Room 02-028, 79110, Freiburg, Germany.
E-mail address: dincer@imtek.de (C. Dincer).

https://doi.org/10.1016/j.bios.2020.112887
Received 23 October 2020; Received in revised form 23 November 2020; Accepted 11 December 2020
Available online 1 January 2021
0956-5663/© 2021 The Authors. Published by Elsevier B.V. This is an open access article under the CC BY license (http://creativecommons.org/licenses/by/4.0/).

2009) with implications in cell proliferation, development and differentiation (Gregory and Shiekhattar, 2005), rendering their downstream characterization highly complex. A way to circumvent this problem is the quantification of not only one but multiple members of a signature cluster of up- or downregulated miRNAs (Xie et al., 2011). In our previous work (Bruch et al., 2019), we combined an electrochemical microfluidic biosensing approach with a clustered regularly interspaced short palindromic repeats (CRISPR)-powered assay, for target amplification-free detection of nucleic acids.

In this study, we employ the *Leptotrichia wadei* Cas13a (Shmakov et al., 2017) for the simultaneous detection and quantitative analysis of different miRNAs of interest. The effector's nuclease activity depends on guidance by a CRISPR-RNA (crRNA) targeting an RNA sequence of interest, upon the recognition of which it collaterally cleaves the single stranded reporter RNAs (reRNAs), provided in its immediate vicinity (Abudayyeh et al., 2016).

Like Chin and colleagues, we create a microfluidic multiplexed lab-on-a-chip (LOC) device by spatially separating multiple immobilization areas within a single channel (Chin et al., 2011), to implement a miniaturized system for highly sensitive electrochemical detection of miRNAs. This approach is faster, cheaper, easier to handle and more economic in terms of sample and reagent consumption (Whitesides, 2006; Yager et al., 2006), compared to the current gold standard for miRNA analysis, which is reverse transcriptase quantitative polymerase chain reaction (RT-qPCR). Another advantage of the method presented here is that it directly provides absolute values, detected in the patient's sample, in contrast to an x-fold in- or decrease in the abundance of the target miRNA detected by RT-qPCR. In our recent work, we presented the first CRISPR/Cas13a-powered electrochemical microfluidic biosensor for on-site miRNA detection, without the need for target amplification (Bruch et al., 2019). Assay calibration revealed the limit-of-detection (LOD) to reside within the low pM-range (2–18 pM, depending on cleavage-time), which makes it applicable to the analysis of real patient's serum samples. In addition, we were able to defy the common conception that signal-off approaches are generally less sensitive than signal-on methods, by showing that the detection limit of our CRISPR-powered assay surpassed the sandwich (signal-on) assay's LOD (1.28 nM) by a factor 1000 (Kutluk et al., 2020). To validate its performance, we compared the results obtained by the CRISPR-powered biosensor to RT-qPCR measurements of the same samples. Here, we introduce the CRISPR-Biosensor X for the simultaneous quantification of multiple miRNAs from a single specimen by combining the single-channel design with a microfluidic stop-flow protocol.

2. Material and methods

2.1. Electrochemical microfluidic multiplexed biosensor

The microfluidic biosensor chip, manufactured based on dry-film photoresist technology according to (Bruch et al., 2017) (see Supporting Material for more information), is divided into two functional units: the incubation area (the microfluidic channel onto the surface of which relevant assay components are immobilized) and the electrochemical cell, consisting of a working electrode (platinum, Pt), a reference electrode (silver/silver chloride, Ag/AgCl) and a counter electrode (Pt), for the amperometric readout. The former spans the following dimensions: 40 or 20 mm in length, respectively, 0.5 mm in width and 64 μm in height. These parameters were optimized by simulations (see Supporting Information) as well as real implementations and are a trade-off between microfluidic dynamics, capacity of biomolecule adsorption and limitations in fabrication (see Chapter 3). By approaching the multiplexing challenge with a single-channel solution (one channel, housing several sequential incubation areas), as shown in Fig. 1, we reduce the number of working electrodes, and thus the required potentiostat channels, to one per channel section in four different designs (Dincer et al., 2019). Formats employed in this study are listed in

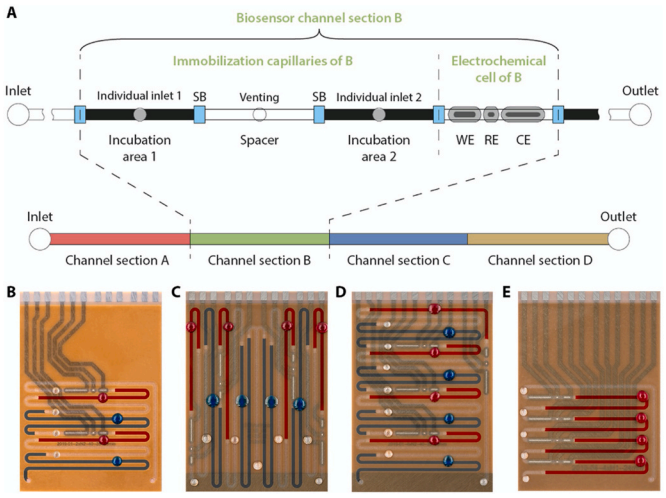


Fig. 1. (A) Illustration of the single-channel multiplexing approach. The top part shows one channel section (green) with two incubation areas (black), separated by a spacer. At the end of each section, an electrochemical cell (grey) performs the amperometric signal readout. To automatically meter the capillary filling of the incubation areas, hydrophobic stopping barriers (blue) are placed between each spacer and incubation area, as well as in front of and behind the electrochemical cell. The lower part displays the entire channel subdivided into four channel sections (SB: stopping barriers, WE: working electrode, RE: reference electrode, CE: counter electrode). (B) - (E) The implemented multiplexed sensor designs: 2xN2, 2x2xN2, 4xN2 and 4xN1 sensors. (For interpretation of the references to colour in this figure legend, the reader is referred to the Web version of this article.)

Table 1
Summary of the key numbers of all multiplexed sensor designs employed in this study. The lengths of the different channel subsections are given in mm (IA: immobilization area, CS: channel section (N), EC: electrochemical cell).

	1st IA (mm)	2nd IA (mm)	Spacer (mm)	# CSs	# ECs
2xN2	40	20	35	2	2
2x2xN2	40	20	34	4	4
4xN2	40	20	34	4	4
4xN1	22	–	–	4	4

Table 1.

In comparison with the parallel channel design employed in our previous work (Kling et al., 2016), the use of a serial design provides superior fluidic control due to a consistent flow rate (which is crucial for flow rate-dependent current signals) and a lower possibility of air bubbles being trapped within the channel. Furthermore, it fits onto an overall smaller layout (19.5 × 28.3 mm) than its predecessor (35.5 × 27.5 mm). These adjustments increase the fabrication density and functional efficiency and hence lower the price per chip (see Supporting Information).

2.2. CRISPR-powered miRNA assay

The concept of our assay builds on the target-recognition induced collateral nuclease activity of the Cas13a/crRNA-complex (see Supporting Video). For its formation, the effector nuclease (preparation according to (Bruch et al., 2019), its target-complementary crRNA (ordered as DNA and reversed, Biomers, Germany) and a murine RNase inhibitor (M0314L, New England BioLabs, Germany) are incubated in Tris-buffer ($MgCl_2$ (6 mM), Tris (40 mM), NaCl (60 mM); pH 7.3) for 15 min at 37 °C. The reRNA (Reporter_RNA_14b_2′OMe-A, Biomers, Germany), labelled with biotin and 6-FAM on the 3′ and 5′-end, respectively, as well as the targets: miR-19b or miR-20a (Biomers GmbH, Germany), are added for a 3-h incubation at the same temperature. Upon

target recognition, the effector is activated and cleaves the reporter RNA (Fig. 2). For information on oligonucleotides used in this study please refer to Supporting Information. Furthermore, the interested reader is referred to (Bruch et al., 2019) for more information on assay design and development as well as the optimization of reagent concentrations, blocking strategy and design of the reRNA and crRNA.

Supplementary video related to this article can be found at https://doi.org/10.1016/j.bios.2020.112887

In the first step, the surfaces of the different immobilization areas are pre-functionalized with streptavidin (0.8 mg ml^{-1} in PBS (10 mM; pH 7.4); S4762-.5 MG, Merck, Germany). Prior to the introduction of the test-solution, the surfaces are blocked with bovine serum albumin (1% in PBS (10 mM, pH 7.4); 126,609-5 GM, ThermoFischer Scientific, USA) to prevent unspecific binding of reagents. This blocking step is necessary since the functionalization of the microchannel is based on physical adsorption of biomolecules to the epoxy-based, negative photoresist (i.e., SU-8) layer of the sensor. Subsequently, the different sample solutions are applied in the respective immobilization areas and in the final incubation step, a glucose oxidase (GOx)-conjugated (for a detailed description of the antibody conjugation see Supporting Information) monoclonal anti-6-FAM antibody (SAB4600050-125UL, Merck, Germany) is introduced. Since the antibody will only bind to the reporter's 6-FAM label, reRNAs cleaved by Cas13a will not contribute to the current signal. Hence, the signal obtained from the enzymatic readout reflects the amount of immobilized GOx and is therefore, inversely proportional to the target concentration in the sample.

The application of bioreagents to the microchannel is conducted and regulated by capillary forces. Thus, propagation of the fluid, applied to the channel inlet, will stop once it reaches a hydrophobic stopping barrier. All incubation steps are followed by a washing step: adding wash buffer (PBS with 0.05% Tween, pH 7.4, P3563, Merck, Germany) into the outlet and applying the vacuum to the inlet of the channel, we remove all unbound biomolecules from the microfluidic channel without contaminating the electrochemical cell. The total processing time required to analyze one patient's sample with the proposed platform amounts to approximately three and a half hours, including about 20 min of hands-on time.

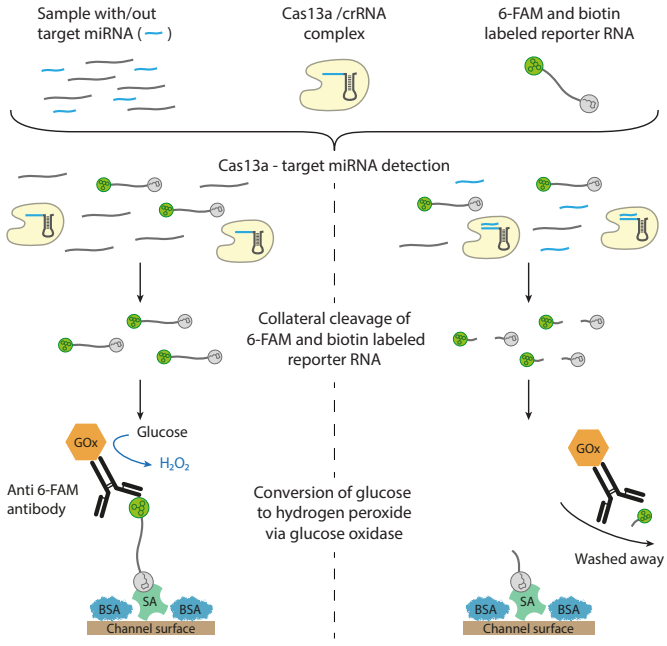


Fig. 2. CRISPR-powered miRNA targeting. In the absence of a target the Cas13a/crRNA complex does not cleave the biotin and 6-FAM labelled reRNA bound to SA on the channel surface, allowing the GOx-conjugated anti-6-FAM-antibody to bind to the 6-FAM label on the reporter and thus enabling enzymatic readout, i.e., the conversion of glucose to hydrogen peroxide (left). In the presence of the target, the reporter is cleaved and no enzymatic labeling takes place (right). The channel surface was coated with SA for reporter binding followed by BSA to prevent unspecific adsorption of biomolecules. (BSA: Bovine Serum Albumin, GOx: Glucose Oxidase, SA: Streptavidin, reRNA: reporter RNA, crRNA: CRISPR RNA, 6-FAM: 6-carboxyfluorescein).

2.3. Electrochemical signal readout

For the electrochemical signal readout, the sensor is placed into a custom-made chip-holder on a printed circuit board (PCB, Beta LAYOUT GmbH, Germany). The inlet and outlet of the microchannel are connected to a syringe pump (PHD 2000; Harvard Apparatus, USA) via silicone (inlet line) and Teflon (outlet line) tubes, respectively. Prior to the measurement, the working electrodes are pre-conditioned to remove manufacturing residues from their surfaces. In this process, the electrode's potential is cycled (5 s at each 0.8 and −0.05 V vs. the on-chip reference electrode) 30 times, while PBS (10 mM, pH 7.4) is passed through the channel and over the electrochemical cell at a flow rate of 20 µl min^{-1}.

In order to perform the amperometic measurement (0.45 V vs. the on-chip reference electrode), a glucose solution (40 mM in PBS (10 mM; pH 7.4); Merck, Germany) is introduced to the microfluidic channel. To amplify the signal peaks, we apply a stop-flow-protocol during which all incubation areas are first filled with the substrate followed by a delay of the flow (5 µl min^{-1}) for 2 min. This allows the enzyme (GOx) to convert the glucose substrate into the electrochemically active hydrogen peroxide, which accumulates within the different incubation areas and, upon restart of the flow, gets oxidized at the respective working electrode. The working electrode is part of the electrochemical cell, which is connected via the PCB to a four-channel potentiostat (MultiEmStat3; PalmSens, The Netherlands). The digital readout of the amperometric signal (Dincer et al., 2016) as well as the pre-conditioning of the working electrodes are performed with the corresponding software (Multitrace 4.3.; PalmSens, The Netherlands).

3. Theory

To approximate the ideal design parameters for the fabrication of a functional single-channel multianalyte biosensor, we developed a 3D geometry (Fig. S1) using the finite element method (COMSOL Multiphysics® 5.3; COMSOL Inc., Sweden) including all essential elements (inlet, outlet, channel width, height and curvature, stopping barriers and area of the working electrode) for the simulation of its microfluidic characteristics. Their respective parameters (Table S1) were hereby kept as close to the actual manufacturing ones as possible. We assume this method to result in a highly realistic prognosis of the chip performance and only very small divergence from the real measurements (Fig. S3) (Bruch, 2020; Dincer, 2016).

For the simulation of the microfluidic dynamics, we used the creeping flow model. The boundary conditions of all channel-walls, other than the SU-8 surface of the immobilization area, were defined as "no flow". The time-dependent, enzyme-based generation of electroactive species (i.e., the conversion of glucose to hydrogen peroxide catalyzed by GOx) flux boundary condition settings are applied to the "Transport of diluted species" model. This transport along the channel is modeled with forced convection to reflect the syringe pump, used in the experimental setup. The simulations were solved on a Windows 10 Enterprise 64-bit platform using an Intel® Core™ i3-5005U processor at 2 GHz with 8 GB RAM.

To investigate possible influences of channel height and flow speed on the microfluidic dynamics, variations of both parameters were simulated (Fig. S3 and Fig. S4). As a result of these simulations, as well as considering fabrication and material limitations, a channel height of 64 µm and flow speeds between 5 and 10 µl min^{-1} were selected as the most suitable combination for stable and reproducible real measurements. The key feature of the design is an optimization of the spacer

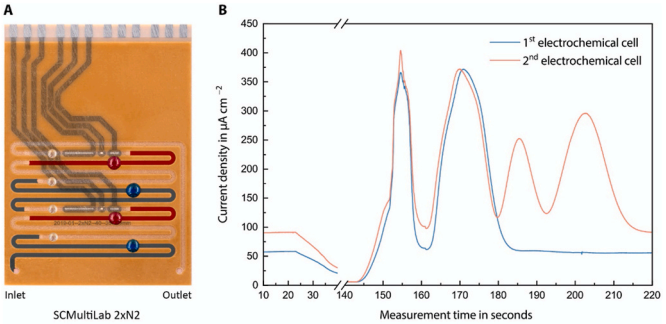
length: On the one hand, it needs to be long enough to guarantee sufficient separation of the successive signals, while on the other hand, it has to be as short as possible to not reduce the peak height of the second signal's peak due to dispersion of the electroactive species (see section *Design Rules and Considerations* in Supporting Information). Simulation of different spacer lengths (20, 25, 33 and 41 mm) revealed 33 mm as the optimum (Fig. S5). Since alteration of the spacer length was not sufficient, we chose to also extend the length of the first immobilization area. Keeping the overall channel length constant, we shifted the ratio (first immobilization area:spacer) to 1.5 and the ratio (first immobilization area:second immobilization area) to 2. These alterations resulted in a clear separation, with the signal reaching the baseline level, between the two identically high peaks, as displayed in Fig. S6.

4. Results and discussion

4.1. The 2xN2 sensor

In order to implement the concept of multiple, spatially separated incubation areas within one microfluidic channel, the 2xN2 sensor chip (Fig. 3A) was designed and manufactured based on parameters optimized in 3D simulations (Fig. S3, S4). The nomenclature of the sensors is derived from the subdivisions of the microfluidic channel: While the first cipher in the name specifies the number of channel sections (N), die second cipher enumerates the number of incubation areas within the respective channel section. The two incubation areas were separated by a 35-mm long spacer and differ in size to counteract unspecific reduction of the second signal peaks by lateral diffusion of the reporter molecule (H_2O_2). The number of electrochemical cells was reduced to only two: one for each channel section (i.e., two incubation areas). To assess its fluidic and mechanical characteristics as well as convenience of readout all incubation areas were functionalized with avidin-coupled GOx (1 µg ml^{-1}) for 1 h at room temperature. Subsequently, the substrate solution (glucose solution, 40 mM) was introduced to the channel and a 2-min stop flow protocol at a flow rate of 5 µl min^{-1} was applied.

The amperometric readout, shown in Fig. 3B displays four signal peaks (two for each electrochemical cell), which can be considered identically high as well as sufficiently separated when taking into account their respective baseline signals. In addition, the clean signal and neat alignment of the first two signal responses of each cell indicate properly working fluidics. As a consequence of the sequential arrangement of the electrochemical cells, the last (in this case the second) cell in the row will measure an approximately two times higher baseline signal



C

	1st BCSR [µA cm-2]	1st BL [µA cm-2]	2nd BCSR [µA cm-2]	2nd BL [µA cm-2]
1st CS	307.80	58.05	310.04	61.55
2nd CS	312.66	91.16	270.88	101.00

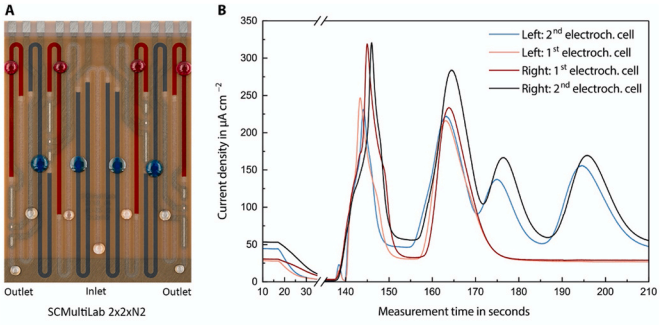
Fig. 3. (A) The 2xN2 sensor houses four incubation areas in two serially arranged channel sections. The incubation areas are functionalized with 1 µg ml^{-1} of avidin-GOx and the 2-min stop-flow protocol is applied at a flow rate of 5 µl min^{-1}. (B) Amperometric signal readout shows almost identical peaks for all incubation areas. (C) Tabular presentation of data collected from the first and second channel sections by their respective electrochemical cells (CS: channel section, BCSR: baseline corrected signal response, BL: baseline signal).

than the first one. This is, presumably, due to the accumulation of electroactive species within the respective incubation areas. Therefore, the signals detected by the first electrochemical cell (blue) are generally slightly lower than the ones measured by the second cell (orange), but this effect is mostly eliminated by subtraction of the baseline signals. The secondary peaks at 186 and 296 s (orange) can be attributed to the hydrogen peroxide from incubation areas non-correspondent to the second electrochemical cell, and therefore, neglected as unspecific.

4.2. The 2x2x2N sensor

Building onto the successful implementation of two serially arranged channel sections, the 2xN2 design was mirrored on the center line of the device to duplicate the total number of incubation areas (Fig. 4A). While the two separate microfluidic channels share a common inlet, each one has its own outlet, connected to individual syringe pumps, to increase fluidic control. Surface functionalization as well as measurement and readout were performed as described for the 2xN2 sensor.

As for the 2xN2 chip version, the baselines recorded by the first electrochemical cells on either side of the chip were approximately half of what was recorded by the subsequent cells (Fig. 4B). However, after baseline subtraction, the signal peaks measured on the left side failed to reach their counterparts from the right. This phenomenon was reproducibly observed for all tested 2x2xN2 sensors and could be due to the fact that the fluidic behavior of the channel on the right side is not ideal. An indication to strengthen this hypothesis is the substantial difference in the signal's response to the stop of substrate flow at 18 s after measurement onset: while there was a sharp drop in the signals measured by the cells on the left side (orange and blue), the signals measured on the right (red and black) only decreased slightly. As a result, there could be a slight but constant flow of substrate solution over the electrochemical cell, which makes the high signal peaks, measured on the right side, even more surprising. In addition, directly after restarting the flow, a small unspecific peak is measured by both electrochemical cells on the left side of the chip. These irregularities and deviations from the ideal fluidic behavior presumably originate in manufacturing imperfections of the channel walls, mechanical bending of the device or small flow variations, introduced by the syringe pump. Such signal behavior has not



C

	1st BCSR [µA cm-2]	1st BL [µA cm-2]	2nd BCSR [µA cm-2]	2nd BL [µA cm-2]
1st CS left	218.72	28.26	185.57	30.73
2nd CS left	186.96	43.62	175.25	46.09
1st CS right	288.42	30.73	200.85	31.92
2nd CS right	266.57	53.86	227.90	55.97

Fig. 4. (A) The 2x2xN2 sensor houses eight incubation areas in four channel sections. The design was accomplished by mirroring the 2xN2 sensor on the central line. All incubation areas are functionalized with 1 µg ml^{-1} of avidin-GOx and the 2-min stop-flow protocol is applied at a flow rate of 5 µl min^{-1}. (B) Amperometric signal readout shows slight shifts along the x-axis (time delay) between the signals as well as small artefacts due to fluidic problems. Also, the signals measured on the right side of the sensor are generally higher than the ones measured on the left. (C) Tabular presentation of data collected from the four channel sections by their respective electrochemical cells (CS: channel section, BCSR: baseline corrected signal response, BL: baseline signal).

been observed in the 2xN2 sensor, but in the 2x2xN2 version small imperfections might have an exaggerated impact on the uniformity of the flow. The design is, therefore, not used for further experiments, but might be a promising alternative, e.g., when implemented with stiffer channel materials.

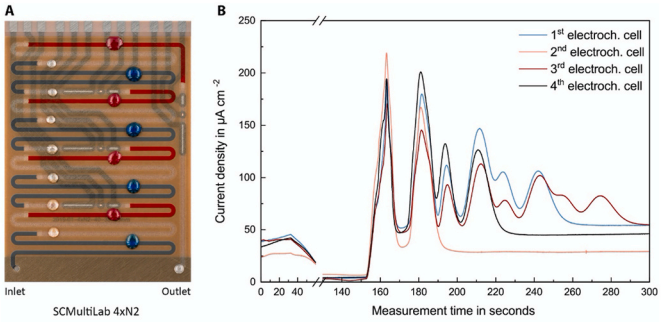
4.3. The 4xN2 sensor

For the 4xN2 sensor chip, the 2xN2 is perpetuated serially to fill the entire chip format and form a single channel, housing a total of eight immobilization areas (Fig. 5A). The notation "4xN2" stems from the structure of the microfluidic channel, incorporating 4 distinct channel sections, each of which houses 2 incubation areas and one spacer. For the dimensions of incubation areas and spacers the same parameters that had already been employed in the 2x2xN2 chip were reused. Surface functionalization as well as measurement and readout were performed as described for the 2xN2 sensor.

Interpretation of the results, however, was not trivial since the four-channel MultiEmStat^3 potentiostat failed to record individual channels (i.e., electrochemical cells), although it is supposed to be able to record on all its channels simultaneously. However, the manufacturer also acknowledges possible recording failures if all electrochemical cells are located in close proximity and immersed in the same electrolyte solution. In this case a sufficient galvanic separation of the channels would not be warranted. We consequently upgraded to a MultiEmStat^3, which features a galvanic isolation module and is capable of recording up to eight channels in parallel without difficulties (Fig. 5B). While the amperometric readout does not display the anticipated distribution of baseline signals, the latter, as well as the recorded signal peaks, show fairly accurate alignment and similar heights. These values provide sufficient similarity to serve as proof-of-principle for the 4xN2 layout. Nevertheless, further measurements and possible tweaks in the stop-flow-protocol are required to develop the device's performance towards an ideal fluidic behavior.

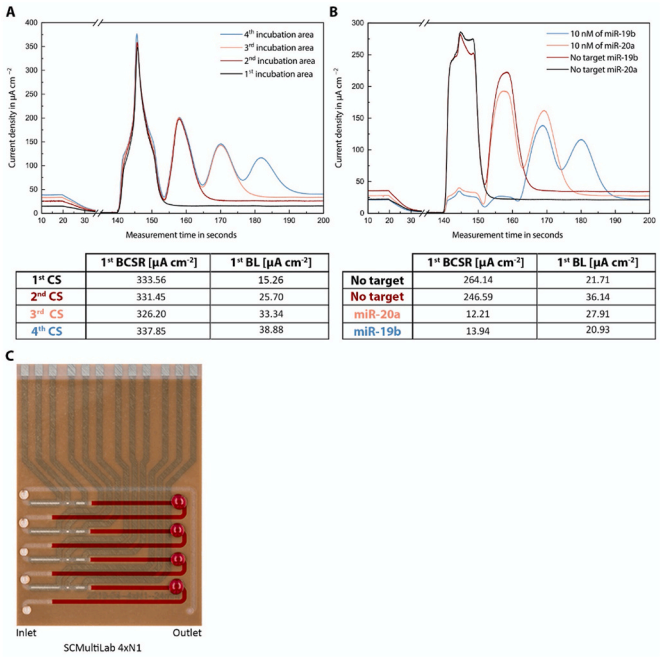
4.4. The 4xN1 sensor

The layout of the 4xN1 sensor chip deviates from the previous versions in that it features no spacers, but each of the four incubation areas is directly followed by its own electrochemical cell, also acting as a spacer in itself (Fig. 6C). These alterations reduce fluidic problems



	1st BCSR [µA cm^{-2}]	1st BL [µA cm^{-2}]	2nd BCSR [µA cm^{-2}]	2nd BL [µA cm^{-2}]
1st CS	148.62	45.38	128.28	51.72
2nd CS	191.91	27.15	133.25	33.63
3rd CS	130.06	40.29	97.91	47.40
4th CS	152.21	42.19	153.98	47.05

Fig. 5. (A) For the 4xN2 sensor, the 2xN2 chip design is serially perpetuated to a total of eight incubation areas. These (two per channel section) are functionalized with 1 µg ml^{-1} of avidin-GOx and the 2-min stop-flow protocol is applied at a flow rate of 5 µl min^{-1}. (B) Amperometric readout reveals close alignment of all primary and secondary signal responses as well as baseline signals. (C) Tabular presentation of data collected from the four channel sections by their respective electrochemical cells (CS: channel section, BCSR: baseline corrected signal response, BL: baseline signal).



	1st BCSR [µA cm^{-2}]	1st BL [µA cm^{-2}]
1st CS	333.56	15.26
2nd CS	331.45	25.70
3rd CS	326.20	33.34
4th CS	337.85	38.88

	1st BCSR [µA cm^{-2}]	1st BL [µA cm^{-2}]
No target	264.14	21.71
No target	246.59	36.14
miR-20a	12.21	27.91
miR-19b	13.94	20.93

Fig. 6. (A) The incubation areas of the 4xN1 sensor are functionalized with 1 µg ml^{-1} of avidin-GOx and the 2-min stop-flow protocol is applied at a flow rate of 5 µl min^{-1} to validate the basic design concept. Signal readout shows simultaneous and almost identical signal peaks for the one-step assay. (B) Multiplexed miRNA measurement of 10 nM of miR-19b in the 4th and miR-20a in the 3rd immobilization area (blue and orange) and without target (first and second immobilization area; red and black) shows a signal drop of 94.88% for 10 nM of target RNA. (C) In the 4xN1 chip design, each channel section houses one incubation area and instead of spacers, each of these is followed by its own electrochemical cell (CS: channel section, BCSR: baseline corrected signal response, BL: baseline signal). (For interpretation of the references to colour in this figure legend, the reader is referred to the Web version of this article.)

originating from very long channel sections (e.g., by lowering the pressure drop) and facilitate interpretation of the readout. Additionally, the length of the incubation areas was extended to 22 mm for a more stable plateau behavior of the signal. Surface functionalization as well as measurement and readout were performed as described for the 2xN2 sensor.

These changes in the design of the multiplexed sensor were proven to be largely beneficial as all four principal signal peaks occur simultaneously and the alignment of the subsequent peaks indicates a properly working stop-flow-protocol without any undesirable flow variations inside the channel (Fig. 6A). As observed in previous chip versions, the hydrogen peroxide gradient that builds up along the length of the microfluidic channel is, again, visible in different levels of baseline signal recorded by the serially placed electrochemical cells. However, after subtraction of the baseline signals the, already fairly similar, principal peaks can be assumed to be identical.

Given the almost ideal fluidic behavior of the 4xN1 design, we further used it for the simultaneous detection of miR-19b and miR-20a (Fig. 6B). To this end the channel was first pre-functionalized with streptavidin and then blocked with bovine serum albumin to prevent unspecific binding of biomolecules. Subsequently, the test solution, containing the effector protein (LwCas13a), the CRISPR-RNA (with the target-complementary guidance sequence), the target miRNAs (miR-19b or miR-20a) and the biotin- and 6-FAM-labelled reporter RNA, was applied to the channel inlets. The amperometric readout was performed as described for the 2xN2 sensor. To simulate the most difficult measurement conditions we measured miR-19b (10 nM) in the fourth and miR-20a (10 nM) in the third incubation area, whereas the first and second incubation areas were tested with test solutions not containing

the targets: elevated baseline levels lead to a decrease in dynamic range and could affect the limit of detection by compression of the standard curve. Using this particular sequence, the first two incubation areas produced 264.14 μA cm^{-2} and 246.59 μA cm^{-2} (baseline subtracted) peaks, leading to substantial baseline levels that were subsequently also measured by the 3rd and 4th cell, which did not produce any signals (12.21 μA cm^{-2} and 13.94 μA cm^{-2}; baseline subtracted). The samples containing the targets provide proof-of-concept for the CRISPR-powered methodology we used for nucleic acid detection, as the reporter RNA was completely cleaved by the successfully activated effector protein.

5. Conclusions

In this study, we successfully validate our CRISPR-powered assay in the simultaneous, spatially separated detection of multiple nucleic acids in a single microfluidic channel using the CRISPR-Biosensor X. The combination of a single channel LOC device for the analysis of up to eight analytes with the stop-flow-protocol has the potential to overcome many technical, like simplicity and sensitivity, and non-technical like costs and acceptance in clinical practice, barriers for multiplexing and thus, to make a great impact on point-of-care diagnostics (for example, hospitals or other settings without well-equipped central laboratories).

The arguably biggest advantage that our bioassay has to offer in terms of multiplexing capabilities is the flexibility to target various RNAs of interest from a single clinical sample using only one effector protein and without changing the sensor or measurement setup. In order to change the analyte, the only component that needs adjustment is the target complementary sequence of the CRISPR RNA. Extension of the existing system for the sake of multiplexing, of course, gives rise to new challenges, like possible cross-reactivity by diffusion between the different incubation areas or increasingly complex chip-fabrication, assay preparation and amperometric readout. We will therefore further focus on optimization of the chip fabrication, development of a standardized readout interpretation and the clinical validation of the CRISPR-Biosensor X.

CRediT authorship contribution statement

Richard Bruch: Methodology, Conceptualization, Validation, Formal analysis, Investigation, Resources, Writing - original draft, Visualization. **Midori Johnston:** Validation, Investigation, Writing - original draft, Visualization. **André Kling:** Methodology, Conceptualization, Writing - review & editing. **Thorsten Mattmüller:** Methodology, Conceptualization, Writing - review & editing. **Julia Baaske:** Methodology, Resources, Writing - review & editing. **Stefan Partel:** Writing - review & editing, Supervision. **Sibylle Madlener:** Writing - review & editing, Supervision. **Wilfried Weber:** Writing - review & editing, Supervision. **Gerald A. Urban:** Writing - review & editing, Funding acquisition, Supervision. **Can Dincer:** Methodology, Conceptualization, Resources, Writing - review & editing, Supervision, Project administration, Funding acquisition.

Declaration of competing interest

The authors declare that they have no known competing financial interests or personal relationships that could have appeared to influence the work reported in this paper.

Acknowledgements

The authors would like to thank the Deutsche Forschungsgemeinschaft (DFG, German Research Foundation) for funding under grant numbers 404478562, 421356369 and 390939984 (EXC-2189), the Austrian Science Fund FWF for funding under the grant number I 3194-B26 as well as Barbara Enderle for technical support and Regina Glatz for help with the experiments.

Appendix A. Supplementary data

Supplementary data to this article can be found online at https://doi.org/10.1016/j.bios.2020.112887.

References

Abudayyeh, O.O., Gootenberg, J.S., Konermann, S., Joung, J., Slaymaker, I.M., Cox, D.B. T., Shmakov, S., Makarova, K.S., Semenova, E., Minakhin, L., Severinov, K., Regev, A., Lander, E.S., Koonin, E.V., Zhang, F., 2016. C2c2 is a single-component programmable RNA-guided RNA-targeting CRISPR effector. Science 80, 353. https://doi.org/10.1126/science.aaf5573.

Bartel, D.P., 2009. MicroRNAs: target recognition and regulatory functions. Cell 136, 215–233. https://doi.org/10.1016/j.cell.2009.01.002.

Bruch, R., 2020. Multiplexed miRNA Biosensor for Pediatric Cancer Diagnostics.

Bruch, R., Baaske, J., Chatelle, C., Meirich, M., Madlener, S., Weber, W., Dincer, C., Urban, G.A., 2019a. CRISPR/Cas13a-Powered electrochemical microfluidic biosensor for nucleic acid amplification-free miRNA diagnostics. Adv. Mater. 1905311. https://doi.org/10.1002/adma.201905311.

Bruch, R., Kling, A., Urban, G.A., Dincer, C., 2017. Dry film photoresist-based electrochemical microfluidic biosensor platform: device fabrication, on-chip assay preparation, and system operation. JoVE 1–7. https://doi.org/10.3791/56105, 2017.

Chen, X., Ba, Y., Ma, L., Cai, X., Yin, Y., Wang, K., Guo, J., Zhang, Yujing, Chen, J., Guo, X., Li, Q., Li, X., Wang, W., Zhang, Yan, Wang, Jin, Jiang, X., Xiang, Y., Xu, C., Zheng, P., Zhang, Juanbin, Li, R., Zhang, H., Shang, X., Gong, T., Ning, G., Wang, Jun, Zen, K., Zhang, Junfeng, Zhang, C.Y., 2008. Characterization of microRNAs in serum: a novel class of biomarkers for diagnosis of cancer and other diseases. Cell Res. 18, 997–1006. https://doi.org/10.1038/cr.2008.282.

Cheng, G., 2015. Circulating miRNAs: roles in cancer diagnosis, prognosis and therapy. Adv. Drug Deliv. Rev. 81, 75–93. https://doi.org/10.1016/j.addr.2014.09.001.

Chin, C.D., Laksanasopin, T., Cheung, Y.K., Steinmiller, D., Linder, V., Parsa, H., Wang, J., Moore, H., Rouse, R., Umviligihozo, G., Karita, E., Mwambarangwe, L., Braunstein, S.L., van de Wijgert, J., Sahabo, R., Justman, J.E., El-Sadr, W., Sia, S.K., 2011. Microfluidics-based diagnostics of infectious diseases in the developing world. Nat. Med. 17, 1015–1019. https://doi.org/10.1038/nm.2408.

Dincer, C., 2016. Electrochemical Microfluidic Multiplexed Biosensor Platform for Point-Of-Care Testing. Dissertation. Univ. Freibg. https://doi.org/10.6094/UNIFR/11053.

Dincer, C., Kling, A., Chatelle, C., Armbrecht, L., Kieninger, J., Weber, W., Urban, G.A., 2016. Designed miniaturization of microfluidic biosensor platforms using the stop-flow technique. Analyst 141, 6073–6079. https://doi.org/10.1039/C6AN01330A.

Dincer, C., Kling, A., Urban, G.A., Bruch, R., 2019. Single-Channel Multianalyte Biosensor. WO 2019/134741 A1.

Filipowicz, W., Bhattacharyya, S.N., Sonenberg, N., 2008. Mechanisms of post-transcriptional regulation by microRNAs: are the answers in sight? Nat. Rev. Genet. 9, 102–114. https://doi.org/10.1038/nrg2290.

Friedman, J.M., Jones, P.A., 2009. MicroRNAs: critical mediators of differentiation, development and disease. Swiss Med. Wkly. 139, 466–472. https://doi.org/10.4414/smw.2009.12794.

Gregory, R.I., Shiekhattar, R., 2005. MicroRNA biogenesis and cancer. Cancer Res 676, 3–22. https://doi.org/10.1007/978-1-60761-863-8_1.

Handy, D.E., Castro, R., Loscalzo, J., 2011. Epigenetic modifications. Circulation 123, 2145–2156. https://doi.org/10.1161/CIRCULATIONAHA.110.956839.

Johnson, R., Zuccato, C., Belyaev, N.D., Guest, D.J., Cattaneo, E., Buckley, N.J., 2008. A microRNA-based gene dysregulation pathway in Huntington's disease. Neurobiol. Dis. 29, 438–445. https://doi.org/10.1016/j.nbd.2007.11.001.

Kling, A., Chatelle, C., Armbrecht, L., Qelibari, E., Kieninger, J., Dincer, C., Weber, W., Urban, G., 2016. Supporting information - multianalyte antibiotic detection on an electrochemical microfluidic platform. Anal. Chem. 88, 10036–10043. https://doi.org/10.1021/acs.analchem.6b02294.

Kutluk, H., Bruch, R., Urban, G.A., Dincer, C., 2020. Impact of assay format on miRNA sensing: electrochemical microfluidic biosensor for miRNA-197 detection. Biosens. Bioelectron. 148, 111824. https://doi.org/10.1016/j.bios.2019.111824.

Miller, B.H., Wahlestedt, C., 2010. MicroRNA dysregulation in psychiatric disease. Brain Res. 1338, 89–99. https://doi.org/10.1016/j.brainres.2010.03.035.

Palanichamy, J.K., Rao, D.S., 2014. miRNA dysregulation in cancer: towards a mechanistic understanding. Front. Genet. 5, 1–10. https://doi.org/10.3389/fgene.2014.00054.

Perdaens, O., Dang, H.A., D'Auria, L., van Pesch, V., 2020. CSF microRNAs discriminate MS activity and share similarity to other neuroinflammatory disorders. Neurol. Neuroimmunol. neuroinflammation 7. https://doi.org/10.1212/NXI.0000000000000673.

Shmakov, S., Smargon, A., Scott, D., Cox, D., Pyzocha, N., Yan, W., Abudayyeh, O.O., Gootenberg, J.S., Makarova, K.S., Wolf, Y.I., Severinov, K., Zhang, F., Koonin, E.V., 2017. Diversity and evolution of class 2 CRISPR-Cas systems. Nat. Rev. Microbiol. 15, 169–182. https://doi.org/10.1038/nrmicro.2016.184.

Whitesides, G.M., 2006. The origins and the future of microfluidics. Nature 442, 368–373. https://doi.org/10.1038/nature05058.

Xie, Z., Wroblewska, L., Prochazka, L., Weiss, R., Benenson, Y., 2011. Multi-input RNAi-based logic circuit for identification of specific cancer cells. Science 80 (333), 1307–1311. https://doi.org/10.1126/science.1205527.

Yager, P., Edwards, T., Fu, E., Helton, K., Nelson, K., Tam, M.R., Weigl, B.H., 2006. Microfluidic diagnostic technologies for global public health. Nature 442, 412–418. https://doi.org/10.1038/nature05064.